NMR and XAS reveal an inner-sphere metal binding site in the P4 helix of the metallo-ribozyme ribonuclease P

Kristin S. Koutmou[a], Anette Casiano-Negroni[a], Melissa M. Getz[a], Samuel Pazicni[a], Andrew J. Andrews[b], James E. Penner-Hahn[a,c], Hashim M. Al-Hashimi[a,c], and Carol A. Fierke[a,b,1]

[a]Departments of Chemistry, [b]Biological Chemistry, and [c]Biophysics, University of Michigan, Ann Arbor, MI 48109

Edited by Jennifer A. Doudna, University of California, Berkeley, Berkeley, CA, and approved December 15, 2009 (received for review June 6, 2009)

Functionally critical metals interact with RNA through complex coordination schemes that are currently difficult to visualize at the atomic level under solution conditions. Here, we report a new approach that combines NMR and XAS to resolve and characterize metal binding in the most highly conserved P4 helix of ribonuclease P (RNase P), the ribonucleoprotein that catalyzes the divalent metal ion-dependent maturation of the 5′ end of precursor tRNA. Extended X-ray absorption fine structure (EXAFS) spectroscopy reveals that the Zn^{2+} bound to a P4 helix mimic is six-coordinate, with an average Zn-O/N bond distance of 2.08 Å. The EXAFS data also show intense outer-shell scattering indicating that the zinc ion has inner-shell interactions with one or more RNA ligands. NMR Mn^{2+} paramagnetic line broadening experiments reveal strong metal localization at residues corresponding to G378 and G379 in *B. subtilis* RNase P. A new "metal cocktail" chemical shift perturbation strategy involving titrations with $Co(NH_3)_6^{3+}$, Zn^{2+}, and $Co(NH_3)_6^{3+}/Zn^{2+}$ confirm an inner-sphere metal interaction with residues G378 and G379. These studies present a unique picture of how metals coordinate to the putative RNase P active site in solution, and shed light on the environment of an essential metal ion in RNase P. Our experimental approach presents a general method for identifying and characterizing inner-sphere metal ion binding sites in RNA in solution.

manganese | ribozyme | RNase P | X-ray absorption spectroscopy | zinc

RNA molecules are large polyanions that associate with numerous divalent metal ions that stabilize their structure and promote catalysis. Identification of the RNA moieties involved in metal-binding and discerning the nature of these interactions is an important outstanding question in the field (1, 2). Whereas RNA-bound metals can be characterized at the atomic level in the solid-state by X-crystallography there are not yet techniques for characterizing the binding sites and coordination schemes for RNA-bound metals in solution. Techniques based on NMR, EPR, and Raman spectroscopy as well as nucleotide analog interference mapping (NAIM) and phosphorothioate substitution exist for identifying RNA residues involved in metal-binding; however the geometry of the bound metal and the nature of the coordination scheme cannot be resolved based on these experiments alone.

RNase P is a metal-dependent ribozyme that catalyzes precursor tRNA (pre-tRNA) maturation by cleaving a specific phosphodiester bond (3). In RNase P, metal ions stabilize the folded RNase P RNA (PRNA) structure, enhance ligand affinity, and stabilize the transition state for cleavage (4); in vivo the metal requirement is fulfilled by Mg^{2+} ions (5, 6). A majority of the ~150 divalent metal ions associated with PRNA bind nonspecifically via electrostatic interactions whereas only a handful of ions form specific contacts with RNase P (5, 7). Discerning the position and structure of the few divalent ions that site-specifically interact with RNA is a major challenge to understanding the structure and mechanism of both RNase P and other ribozymes (1–3).

Many large ribozymes, including group I and II introns and RNase P, require structural, catalytic and cocatalytic metal ions (2). Catalytic metals directly participate in the cleavage reaction, whereas cocatalytic metals are required for catalysis, but do not directly stabilize the chemical transition state. Divalent metal ions can contact RNA via either outer- or inner-sphere interactions (8). Outer-sphere interactions are water-mediated, whereas inner-sphere interactions involve direct coordination of metal ions by RNA functional groups. Analysis of the Mg^{2+} dependence of RNase P in cobalt hexamine ($Co(NH_3)_6^{3+}$) reveals at least two classes of inner-sphere-coordinated metal ions required for catalytic activity: one class stabilizes the active RNase P•pre-tRNA conformation and another class enhances cleavage (7). There is also evidence that additional outer-sphere metal ions enhance RNase P reactivity (7, 9). Kinetic isotope effect studies of PRNA-catalyzed cleavage suggest that a metal-bound water functions as the nucleophile in the hydrolytic reaction (6). Although several sites have been implicated in metal-binding, the divalent metal-binding sites essential for catalysis and ligand binding have not yet been well characterized in PRNA (3).

Helix P4 is the most highly conserved region of the catalytic PRNA retained in all three domains of life, possessing 11 of the 21 universally conserved PRNA nucleotides (10). Additionally, helix P4 is positioned in the core of the enzyme (4, 11). Mutation of single nucleotides in the P4 helix reduces RNase P activity by >100-fold in vitro, and inhibits cell growth under conditions of magnesium starvation (12–14). Furthermore, phosphorothioate modifications of nonbridging oxygens in the P4 helix, particularly at A49 and A50 in *B. subtilis* PRNA (A67 and A68 in *E. coli*), decrease catalytic activity up to 10,000-fold with minimal affects on pre-tRNA affinity (14–16). Some of these catalytic defects can be rescued by adding Mn^{2+}, suggesting that metal ions form an inner-sphere contact with the P4 helix phosphodiester backbone (3, 14, 15). Cross-linking studies examining the position of the pre-tRNA cleavage site relative to helix P4 suggest that metal-binding in helix P4 leads to indirect stabilization of catalytic metal ions at the scissile phosphate (17). Thus, helix P4 is a likely region for catalytic and/or cocatalytic metal ion binding sites, and for containing a portion of the active site (15, 17). Although biochemical evidence has demonstrated that several divalent metal binding sites crucial to catalysis are located in P4, thus far it has been impossible to characterize the molecular level structure of these sites.

Author contributions: K.S.K., A.C.-N., M.M.G., S.P., A.J.A., J.E.P.-H., H.M.A.-H., and C.A.F. designed research; K.S.K., A.C.-N., M.M.G., S.P., and A.J.A. performed research; K.S.K., A.C.-N., M.M.G., S.P., J.E.P.-H., H.M.A.-H., and C.A.F. analyzed data; and K.S.K., A.C.-N., M.M.G., S.P., J.E.P.-H., H.M.A.-H., and C.A.F. wrote the paper.

The authors declare no conflict of interest.

This article is a PNAS Direct Submission.

[1]To whom correspondence should be addressed. E-mail: fierke@umich.edu.

This article contains supporting information online at www.pnas.org/cgi/content/full/0906319107/DCSupplemental.

Anomalous scattering in diffraction analysis (3.5 Å resolution) of *B. stearothermophilus* PRNA crystals soaked in metals has identified a number of possible metal ion binding sites in RNase P (18). Of these, four osmium(III) hexamine (a $Mg(H_2O)_6^{2+}$ mimic) and two metal-binding sites (Pb^{2+}, Sm^{3+}, Gd^{3+}, and Yb^{3+}) are in the P4 helix near residues A48, A49, G50, G378, and G379 in PRNA (*B. subtilis* numbering). Coordination contacts to these metals have been proposed based on electrostatic calculations; however, the resolution of these data is insufficient to distinguish between inner and outer-sphere coordination. Additionally, previous NMR studies of a mimic of the P4 helix from *B. subtilis* revealed association of Mg^{2+} at residues corresponding to A49, G378, and G379 in PRNA (19), providing further evidence for metal-binding in RNase P helix P4.

Here we present a unique strategy that combines NMR and X-ray absorption (XAS) spectroscopy to identify and characterize RNA-metal interactions. The method is applied to a stem-loop RNA that serves as a model for the *B. subtilis* RNase P helix P4 (nucleotides 48–57 and 391–398). These two biophysical techniques are complementary, as NMR can identify nucleotides that are located near metals, whereas XAS can characterize the nature of the interactions involved, including distinguishing between inner and outer-sphere metal coordination. We also use a metal cocktail NMR chemical shift perturbation approach for resolving inner- versus outer-sphere interactions, and to corroborate the XAS results. Our approach takes advantage of the fact that RNase P is active in vitro in the presence of a variety of divalent metal ions (Mg^{2+}, Ca^{2+}, Mn^{2+}, and $Zn^{2+}/Co(NH_3)_6^{3+}$) (20, 21). XAS data indicate that Zn^{2+} is involved in inner-sphere interactions with the P4 helix mimic and that the bound Zn^{2+} exhibits six-coordinate geometry with an average Zn^{2+}-O/N bond distance of ~2.08 Å. The NMR studies provide evidence for a strong association that is consistent with inner-sphere divalent metal-binding at a site located near G22 and G23 in the *B. subtilis* P4 helix model (G378 and G379 in full-length *B. subtilis*). This work represents the successful combination of NMR and XAS for studying metal coordination by RNA, and should be applicable to the study of other metal-requiring ribozymes. Furthermore, the study of the inner-sphere metal-binding site identified in helix P4 not only provides a molecular level characterization of the environment of a catalytic and/or cocatalytic metal ion in RNase P, but also suggests that tandem guanosines adjacent to a bulged nucleotide could be a general metal ion binding motif in RNA (22, 23).

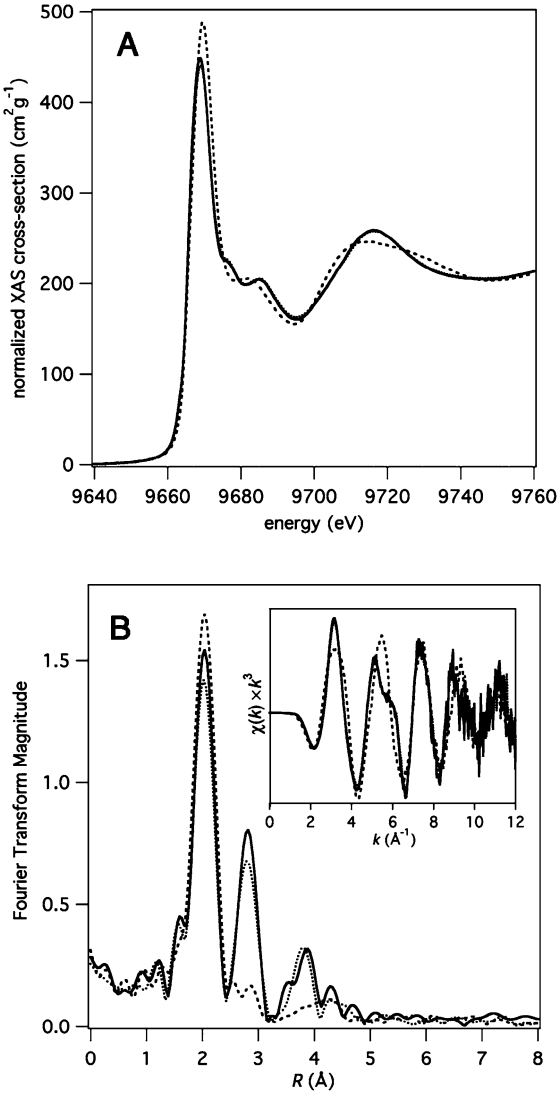

Fig. 1. XAS (*A*) Normalized K-edge XANES spectra of Zn^{2+} in the presence and absence of P4. (*B*) Phase-corrected FTs of the EXAFS spectra of Zn^{2+} in the presence and absence of P4. (*Inset*) k^3-weighted EXAFS spectra of Zn^{2+} in the presence and absence of P4. Spectra from duplicate Zn^{2+} – P4 samples are shown in *Solid* and *Dotted Lines*, whereas the Zn^{2+} alone control spectra is a *Dashed Line*.

Results

XAS Reveals Inner-Sphere Binding of Zn^{2+} to Helix P4. X-ray absorption near edge structure (XANES) and extended x-ray absorption fine structure (EXAFS) are metal-specific techniques that provide information about the average ligand environment of metals. These techniques are especially useful for investigating the structures of Zn^{2+} and other d^{10} metals that are silent in other spectroscopic methods (24). Large RNAs bind multiple metal ions, a situation that usually renders XANES and EXAFS uninformative, as XAS data report on an average metal environment. Here, however, we have devised a strategy to probe a metal site that can be mainly populated at low concentrations of metal ions. XAS provides structural information regarding both the first coordination sphere and the environment beyond the immediate coordination metal ligands. Though XAS has previously been used to study metal coordination to DNA (25, 26), we believe this work represents a unique application of XAS techniques to the study of metals bound to RNA.

The normalized XANES spectra for Zn^{2+} in the presence and absence of RNA (Fig. 1*A*) were measured in the presence of $Co(NH_3)_6^{3+}$ that competes with Zn^{2+} mainly for outer-sphere interactions with RNA (27). The spectra are significantly perturbed by the addition of P4, indicating a change in the Zn^{2+} coordination environment relative to the buffer control. Whereas these differences are difficult to relate directly to specific structural changes, they are strong evidence that zinc binds to the helix P4 mimic.

The EXAFS data confirm that the P4 RNA construct alters the coordination environment of Zn^{2+} (Fig. 1*B*). The first-shell scattering (peak at R = ~2.0 Å) is nearly identical for all samples; the larger peak for the control suggests that there may be slightly more disorder in bond lengths for the Zn^{2+}-P4 samples. In contrast to this similarity, the Zn^{2+}-P4 samples show pronounced outer-shell scattering (at R = ~2.8 Å, ~3.8 Å) that is not seen for the control. Because these peaks can arise only from non-water ligands bound to the Zn^{2+}, they provide direct evidence for an inner-sphere contact between Zn^{2+} and the P4 construct.

Fits to the EXAFS data are summarized in Table 1 and illustrated in the supporting information (Figs. S1–S3). The nearest-neighbor scattering is best fit as six oxygen or nitrogen scatterers at an average Zn^{2+}-O/N distance of 2.08 Å for the Zn^{2+}-P4 samples and 2.07 Å for the control. Although the next-nearest neighbor peaks (R = ~2.8 Å) can be fit with either phosphorous or zinc scattering,

the best and most chemically-reasonable fits based on the structure of the P4 helix are obtained by using a single shell of low-Z (C/N/O) scatterers at an average distance of ~2.93 Å (Tables S1, S2 and *Discussion*). No attempt was made to fit the $R = \sim 3.8$ Å peak. The fits of the Zn^{2+}-P4 data are most consistent with Zn^{2+} coordinating to one or more of the bases of the P4 helix via an inner-sphere mechanism.

Probing P4 Metal Localization Using Mn^{2+} Paramagnetic Line Broadening. We used NMR to pinpoint the location of the inner-sphere metal ion identified by XAS. Previous NMR chemical shift mapping experiments on the *B. subtilis* RNase P P4 helix stem-loop model revealed significant association of Mg^{2+} ions at the P4 major groove near the flexible pivot point (A5, G22, and G23) (Fig. 2*A*) corresponding to residues in PRNA that biochemical experiments have previously implicated as binding catalytically important metals (19). However, chemical shift changes can result from metal ion localization and/or structural changes. To further characterize the metal-binding site in P4, we used line broadening experiments to identify sites that are proximal to bound Mn^{2+}. Mn^{2+} is a paramagnetic ion that induces distance-dependent (r^{-6}) line broadening in the resonances located near the metal ion. Furthermore, Mn^{2+} can functionally substitute for Mg^{2+} in RNase P in vitro (20). Incremental addition of $MnCl_2$ from 3–60 μM increases the line broadening of several resonances in 2D HSQC spectra of P4 (Fig. 2). The broadening is particularly pronounced for G22 followed by residues G23 and A3–G6. Interestingly, these are the same residues that exhibit the largest Mg^{2+} chemical shift perturbations (19) (Fig. 2). Together with the EXAFS data, these results strongly suggest that a metal ion interacts via inner-sphere coordination with RNA ligands in the major groove of P4 near residue G22.

Resolving Inner From Outer-Sphere Interactions: Chemical Shift Changes Induced By Adding $Co(NH_3)_6^{3+}$/Zn^{2+}. Mn^{2+} line broadening cannot discern which RNA ligands form outer- versus inner-sphere interactions with divalent metal ions. This question was addressed by performing chemical shift perturbations with a combination of metal ions. $Co(NH_3)_6^{3+}$ and Zn^{2+} were employed to mimic outer- and inner-sphere interactions of Mg^{2+}, respectively (27). Although RNase P has no catalytic activity in the presence of $Co(NH_3)_6^{3+}$ alone (despite formation of a RNase P•pre-tRNA complex), the activity increases upon addition of either Mg^{2+} or Zn^{2+} (21). Under these conditions, we used NMR chemical shift perturbations to analyze the location of the inner-sphere Zn^{2+} metal observed by XAS.

Significantly less $Co(NH_3)_6^{3+}$ (500 μM) is needed to induce chemical shift perturbations comparable in size to those induced by Mg^{2+} (15 mM), as reported previously (28). This is expected

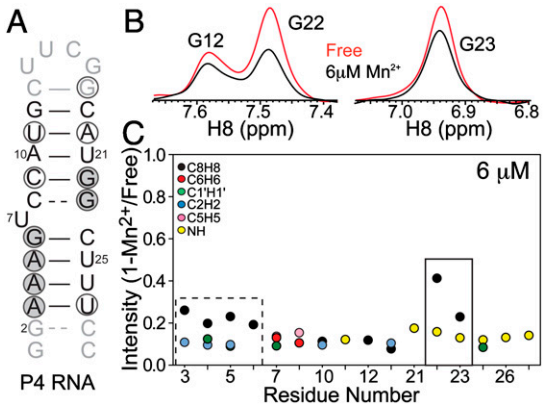

Fig. 2. Metal localization in P4 detected by Mn^{2+}. (*A*) Secondary structure of P4. Highlighted are the residues with $K_{d,app}$ values of 1–4 mM for Mg^{2+} (*Open* and *Filled Circles* except for G6) and significant Mn^{2+} broadening (*Filled Circles*). (*B*) 1D spectra of sites in P4 in the absence (*Red*) and presence (*Black*) of 6 μM Mn^{2+}. (*C*) Normalized intensities ($=1 - I_M/I_F$) upon addition of 6 μM Mn^{2+} are shown as a function of residue number for the following vectors: C8H8 (*Black*), C6H6 (*Green*), C1′H1′ (*Red*), C5H5 (*Blue*), C2H2 (*Pink*), and N1H1/N3H3 (*Yellow*). Highlighted are the residues with the greatest broadening (*Solid Line Box*) and a second group with high broadening (*Dash Line Box*).

because $Co(NH_3)_6^{3+}$ has a higher charge than Mg^{2+} (28); similarly, lower concentrations of $Co(NH_3)_6^{3+}$ compared to Mg^{2+} are required to stabilize the PRNA structure (7, 21). Whereas Mg^{2+} perturbations include specific residues above and below the U7 bulge, $Co(NH_3)_6^{3+}$ induces shifts in the bulged U7 as well as in a larger number of residues above and below this nucleotide (Fig. S4). To determine if the mode of binding is different for Mg^{2+} and $Co(NH_3)_6^{3+}$, the directions of the chemical shift perturbations in the HSQC spectra were carefully compared. Whereas similar perturbation directions are observed for the majority of the resonances, consistent with outer-sphere coordination, there is a group of resonances that exhibit clear differences. Remarkably, these resonances ($G23_{C8H8}$, $G23_{N1H1}$, and $G22_{C8H8}$) (Fig. 3) are the same resonances that exhibit the largest Mg^{2+} chemical shift perturbations (19) and Mn^{2+} line broadening (Fig. 2). Whereas differences are also observed for $A10_{C8H8}$, this resonance does not show significant Mg^{2+} perturbations or Mn^{2+} line broadening. Thus, distinct NMR experiments consistently suggest that G23 and G22 bind metals differently from other regions in P4. One possibility is that a metal ion binds at these sites via inner-sphere interactions that cannot be accomplished by $Co(NH_3)_6^{3+}$.

It is possible that Zn^{2+} restores the catalytic activity of RNase P in the presence of $Co(NH_3)_6^{3+}$ by fulfilling the requirement for

Table 1. EXAFS fitting results*†

			First shell: O/N			Second shell: O/N			Second shell: C			
Sample	N_{idp}‡	N_{var}	CN	R(Å)	$\sigma^2 \times 10^3$	CN	R(Å)	$\sigma^2 \times 10^3$	CN	R(Å)	$\sigma^2 \times 10^3$	ξ'§
Zn + P4(1) ¶	10.5	5	6	*2.078*	*8.2*	—	—	—	*7.88*	*2.928*	*7.1*	15.8
$k = 2.6 - 15.5$		5	6	*2.078*	*8.1*	*5.54*	*2.872*	*7*	—	—	—	14.6
$R = 1.5 - 3.2$		8	6	*2.078*	*8.1*	2.52	*2.83*	*1.1*	*2.96*	*2.994*	*1.1*	30.5
Zn – MES(2)¶	10.6	2	6	*2.069*	*6.2*	—	—	—	—	—	—	6.35
$k = 2.5 - 12.3$		—	—	—	—	—	—	—	—	—	—	—
$R = 1.5 - 3.2$		—	—	—	—	—	—	—	—	—	—	—

*Fitting parameters that were varied are denoted in italics.
†The CN of the first shell was fixed at six, as the range of fitted distances is consistent with a six-coordinate Zn^{2+}, as determined by valence bond sum analysis.
‡N_{idp} is the number of independent data points in the region of the Fourier transformed spectrum where the data are physically meaningful. The equation $N_{idp} = (2\Delta k \Delta R)/\pi$ yields N_{idp} as a conservative estimate for all above samples.
§ξ', mean-square deviation between the k^3-weighted data and fit divided by $N_{idp} - N_{var}$ where N_{var} is the number of variables in the fit. ξ' values provide a partial correction for the fact that more parameters invariably give better fits (36).
¶Sample 1: 2 mM P4, 2 mM Zn^{2+}, and 2 mM $Co(NH_3)_6^{3+}$; sample 2: 2 mM Zn^{2+}.

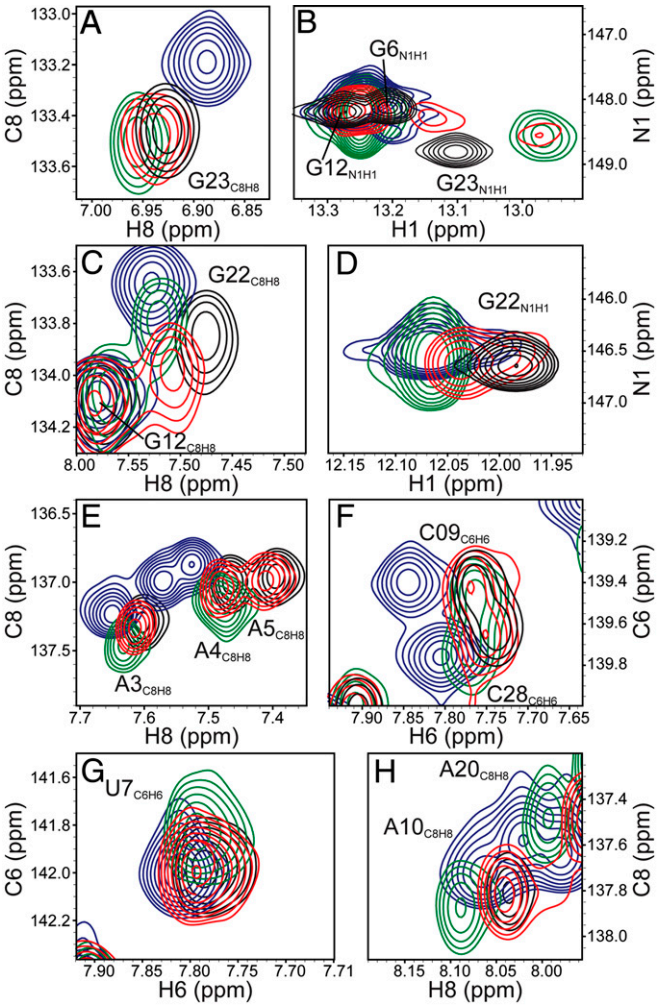

Fig. 3. Detection of inner-sphere binding sites in P4 in $Co(NH_3)_6^{3+}/Zn^{2+}$. The aromatic and imino region of a two-dimensional HSQC spectrum showing sites in P4 in the absence (*Black*) and presence of: 15 mM Mg^{2+} (*Blue*), 0.5 mM $Co(NH_3)_6^{3+}$ (*Green*), and 0.2 mM $Co(NH_3)_6^{3+}$/1 mM Zn^{2+} (*Red*). All experiments were performed at pH 6.2 with 10 mM NaCl, and 10 mM NaH_2PO_4.

this inner-sphere P4 coordinated metal. To test this hypothesis, we performed chemical shift perturbation using Zn^{2+} in the presence and absence of $Co(NH_3)_6^{3+}$ (Fig. 3). In the absence of $Co(NH_3)_6^{3+}$, most peaks do not shift significantly upon addition of 16 mM Zn^{2+}; the main exception is residue G22 that shows $\geq$0.04 ppm changes in chemical shifts (Fig. S4*B*). Similar zinc-induced chemical shift perturbations are observed at a lower zinc concentration (1 mM) in the presence of 0.2 mM $Co(NH_3)_6^{3+}$ (Fig. S4*C*). Interestingly, many perturbations involving residues A3-G6 act to restore the "metal-free" spectrum of P4 (Fig. 3), suggesting that the addition of Zn^{2+} causes $Co(NH_3)_6^{3+}$ to be displaced at these sites.

At two sites, G23 (N1H1) and G23 (C8H8), the addition of Zn^{2+} causes chemical shift changes from a unique position observed in $Co(NH_3)_6^{3+}$ toward that observed in Mg^{2+} (Fig. 3). This provides further evidence that G23 coordinates an inner-sphere divalent metal ion. Interestingly, two resonances are observed for the peak at G23 (N1H1) in $Co(NH_3)_6^{3+}/Zn^{2+}$ suggesting slow exchange between a Zn-bound and Zn-free species, consistent with high-affinity metal binding. Residue G22 shows unusual chemical shift perturbations that could also be consistent with inner-sphere coordination (Fig. 3*C*). For G22 (N1H1), we observe a major and a minor peak, with the major peak having a position consistent with the Mg^{2+}-"bound" spectra. For G22 (C8H8), a unique perturbation direction is seen that may reflect a new environment. It is plausible that the P4 spectra in $Co(NH_3)_6^{3+}/Zn^{2+}$ do not perfectly mirror those of Mg^{2+} even if similar RNA ligands are involved in inner-sphere coordination with metals. Zn^{2+} clearly has a unique effect on G22; this site shows significant chemical shift perturbations upon addition of Zn^{2+} and Mg^{2+} alone, and exhibits the strongest Mn^{2+} linewidth broadening. Finally, the resonances for residues U11-C19 do not shift upon the addition of Zn^{2+} to the P4 mimic in $Co(NH_3)_6^{3+}$ suggesting either that RNA-metal interactions do not occur, or that the interactions with $Co(NH_3)_6^{3+}$ and Zn^{2+} are comparable (Fig. 3*B* and *F*).

Furthermore, the structurally benign mutation involving the swapping of the C8/G23 base-pair into a G8/C23 base-pair in the P4 model helix results in very different Mg^{2+} chemical shift perturbations (Fig. S5). Most notable is the loss of chemical shift perturbations at G22 and the appearance of perturbations in bulge residue U7. These data indicate that the metal binding mode is altered and shifted towards the bulge and residues in the lower stem, therefore, suggesting that the tandem G22 and G23 residues in the upper P4 stem impart a unique Mg^{2+} binding site in RNase P. Furthermore, it is possible that a similar metal-binding motif may be used in other ribozymes.

Discussion

The molecular characterization of RNA-metal binding under solution conditions is a long-standing problem that precludes a complete understanding of how RNA structures fold and function at the atomic level. Here, we introduce a unique approach for probing RNA-metal binding in solution that combines NMR and XAS. By using this approach, we characterized metal binding with the P4 helix mimic of RNase P. Although the metal requirement of RNase P is well documented, the PRNA nucleotides that form inner-sphere interactions with metals, and the nature of these interactions, are poorly understood. Our study identifies and characterizes an inner-sphere metal binding site in P4 that is a potential catalytic/co-catalytic site in PRNA. The *B. subtilis* P4 helix mimic used in our study adopts a conformation that is similar to that observed in the crystal structure of the full-length *B. stearothermophilus* ribozyme (19) and, thus, some of the unique metal binding properties of full-length RNase P may be reflected in this truncated mimic.

The nucleotides we report to directly coordinate divalent metal ions (G22 and G23 in Fig. 2*A*) were previously identified as metal binding sites in the initial NMR structures of helix P4 from *E. coli* and *B. subtilis* (19, 28). However, because the first structures were solved in the presence of either Mg^{2+} or $Co(NH_3)_6^{3+}$ ions, but not the presence of both ions, it was not possible to probe whether the metal-binding sites form inner-sphere or outer-sphere coordination interactions.

Inner-sphere metal-binding site. The identification of the tandem purines, G22 and G23, as an inner-sphere metal-binding site is consistent with other metal sites observed in RNA. For example, metals binding to tandem purines are seen in crystal structures of human SRP, hammerhead ribozyme, and the leadzyme (22, 29, 30), suggesting that this may be a general metal binding motif in RNA. A possible model for the observed metal-binding site in P4 is presented in Fig. 4. In this model, the inner-sphere ligands of the octahedral metal are: the O6 moieties of G22 and G23 and four water molecules. Two of these water molecules hydrogen bond with the N7 groups of these two bases. The remaining two zinc water ligands are positioned to potentially interact with the bases of G6 and U21. The line broadening by Mn^{2+} of the C8H8 peak at G6, G22, and G23 support this model. Likewise, the large chemical shift changes upon addition of Zn^{2+} and/or Mg^{2+} for the C8H8 and N1H1 atom pairs of G22 and G23 support the proposed metal-water hydrogen bonds with N7 (Figs. 2 and 3). Finally, the C6H6 peak of U21 also shows a chemical shift

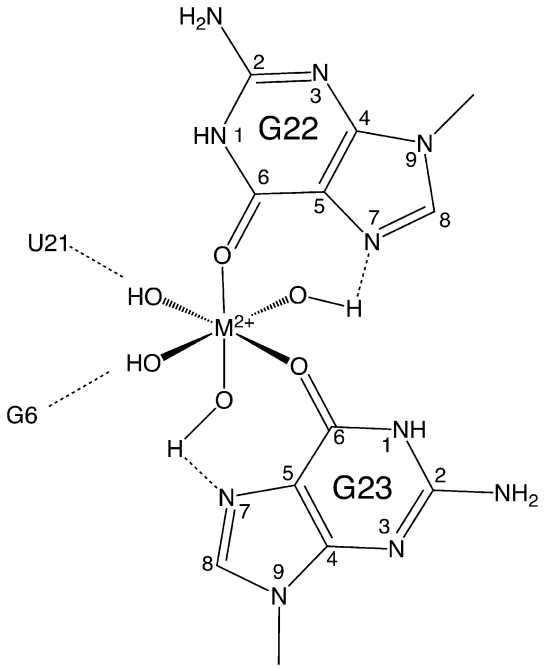

Fig. 4. Proposed model of inner-sphere metal-binding site in P4 with inner-sphere coordination by G22 and G23. This model best fits both the NMR and the EXAFS data indicating that zinc coordinates to this site in the P4 mimic in a six-coordinate geometry.

change upon addition of Zn^{2+} suggestive of an interaction with the bound metal ion (Fig. S4). Unfortunately, no information on the O6 position could be obtained from the NMR data in this study to provide further verification of inner-sphere interactions with this moiety.

The proposed model is strikingly similar to a metal site recently reported in the crystal structure of a group I intron fragment, in which the O6 and N7 moieties of guanosine form inner, and outer-sphere interactions, resp., with a hydrated magnesium ion (31). Furthermore, the recent structure of a truncated *B. stearothermophilus* RNase P RNA with the outer-sphere Mg^{2+} mimic Os(III)hexamine revealed a metal binding site within 6 Å of the corresponding A3, A4, G6, G22, and G23 positions in the P4 helix mimic (18). This result suggests that a metal binds near G22/G23, however, the resolution of the X-ray data does not allow for the elucidation of specific metal-nucleotide contacts. Although tandem purines have previously been identified as metal binding sites in RNA (22), the data from P4 suggest that the dynamic nature of the G23-C8 base-pair adjacent to the U7 bulge (19) promotes specific, inner-sphere metal ion binding. Thus, we hypothesize that stacked tandem C-G base-pairs above a bulged pyrimidine may help to promote inner-sphere metal ion binding in RNAs.

The XAS data are also consistent with the model in Fig. 4. The nearest-neighbor interactions are consistent with exclusively low-*Z* (O or N) ligands at an average distance of 2.08 Å. The apparent EXAFS coordination number is six and bond-valence-sum calculations (32) support the conclusion that the Zn is six-coordinate (note that the Zn-O and Zn-N values in ref. 32 are reversed), as does the similarity between the XANES spectra for Zn-P4 and Zn^{2+}. The outer-shell scattering provides direct evidence that one or more water ligands have been replaced with an RNA-derived ligand and the apparent Zn-C distance of ~2.93 Å is consistent with the model shown in Fig. 4. It is difficult to provide unambiguous interpretations for outer-shell scattering for sites, such as this, where the ligation is expected to be heterogeneous. Alternate explanations for the ~2.9 Å peak could be: (*i*) a phosphorous atom from the RNA phosphodiester backbone, and the data can be modeled with one Zn-P at ~2.66 Å and ~5 Zn-C at 2.93 Å; or (*ii*) a $Zn_2(\mu\text{-}OH)_2$ cluster; the best fit for such a model gives a Zn-Zn distance of ~2.85 Å and a Zn-C distance of ~2.99 Å. However, both of these models predict Zn-P or Zn-Zn distances that are shorter than typically seen in model compounds and they are difficult to reconcile with the NMR data. Therefore, the inner-sphere metal-binding site shown in Fig. 4 is the model that is most consistent with all of the NMR and XAS data. XAS and NMR have been combined uniquely to gather structural information on metals bound to RNA, and this approach can be used in the future to provide valuable insight into other RNA systems.

Function of Metal Site. There are a number of potential roles for the inner-sphere metal-binding site at G22 and G23. Given that the P4 helix in PRNA binds metal ions required for catalysis, this could be the catalytic metal site. Alternatively, it is also possible that the G22/G23 site is a cocatalytic metal site, and/or that the inner-sphere associated metal ion stabilizes PRNA in the active conformation. Phosphorothioate rescue and cross-linking studies indicate that a P4 helix metal-mediated interaction with pre-tRNA helps to set-up the active site for coordination of the catalytic metal ion (15, 17). Mutagenesis studies at these positions in full-length PRNA demonstrate that this region is important for the metal-dependent activity of RNase P (13). Therefore, it is likely that this inner-sphere metal site in P4 contributes to enhancing the RNase P activity in a significant way.

We have seen that P4 has the potential to bind inner-sphere metals based on the binding properties of the site deduced by biochemical data. NMR chemical shift mapping in the presence of a combination of Mn^{2+}, $Co(NH_3)_6^{3+}$, and Zn^{2+}, together with EXAFS, promises to be a ubiquitous method for assigning and characterizing outer- and inner-sphere metal-binding sites in a variety of RNAs.

Materials and Methods

Preparation and Purification of RNA. P4 samples (Fig. 1*A*) for XAS studies were prepared by in vitro transcription reactions by using T7 RNA polymerase, and synthetic DNA templates containing the T7 promoter (33) and sequence of interest. RNA transcripts were purified on denaturing PAGE gels, passively eluted, concentrated in Amicon Ultra-Concentrators (5,000 MWCO), and precipitated with ethanol. The samples of RNA (1 mM) contained: 50 mM MES, 10 mM $NaNO_3$, 500 μM $ZnSO_4$, 500 μM $[Co(NH_3)_6]Cl_3$, and 30% glycerol. P4 samples for NMR studies were transcribed by using uniformly $^{13}C/^{15}N$ labeled nucleotides (Spectra Stable Isotopes, Inc). The samples of RNA (100–500 μM) contained 10 mM NaCl, 10 mM sodium phosphate, pH ~ 6.2, and other ions, as indicated. No metal-phosphate precipitates were observed during the experiments.

XAS Spectroscopy and Data Analysis. RNA samples were loaded into Lucite cuvettes with 40 μm Kapton windows and frozen in liquid N_2. XAS data were collected at Stanford Synchrotron Radiation Lightsource (SSRL) on beamline 9–3, as described previously (34). Average files for Zn-RNA and Zn alone samples were calculated by using 10 scans and 4 scans, resp. For further experimental parameters, see Table S3. XANES data were normalized by fitting the McMaster absorption coefficients below and above the edge to the data by using a single background polynomial and scale factor (35, 36). The EXAFS background removal used a three-region, cubic spline. The data were converted to *k* space by using $E_0 = 9664$ eV (37), curve fitting details are provided in Table S3 (34). The program Feff v7.02 (38) was used to calculate amplitude and phase functions, for a Zn-O interaction at 2.0 Å, and Zn-P, Zn-C, and Zn-Zn interactions at 3.0 Å. Data were analyzed in *k* space by using the program EXAFSPAK (39). For all data, S_s was fixed at 0.9 based on fits to the EXAFS data for structurally characterized model complexes (37, 40).

NMR Spectroscopy. NMR experiments were carried out on an Avance Bruker 600 MHz NMR spectrometer equipped with a triple-resonance 5 mm cryogenic probe at 298 K in Shigemi tubes (~300 μL). Two-dimensional $^{13}C^1H\,S^3E$ HSQC experiments (41, 42) were used to monitor chemical shift changes. NMR spectra were processed using NMRPipe/NMRDraw (43),

analyzed using NMRView (44), and overlaid using SPARKY 3. The magnitude of metal-induced chemical shift-perturbations were quantified by using $\Delta\delta = \sqrt{(\Delta\delta_H)^2 + (\alpha\Delta\delta_X)^2}$ (19), where δ_H and δ_X are the changes in proton and carbon/nitrogen chemical shift and α is the ratio of the C/N and H gyromagnetic ratio (Fig. S5). Data from terminal and apical loop residues were excluded from the analysis. For the Mn^{2+} line broadening experiments, two-dimensional HSQC spectra were recorded on the $^{13}C/^{15}N$-labeled P4 stem-helix RNA sample (130–500 μM) following the addition of 3 μM, 6 μM, 12 μM, 24 μM, and 60 μM Mn^{2+}. The intensity for each type of C-H and N-H spin measured in Mn^{2+} was normalized to $1 - I_M/I_F$ (I_M and I_F are the peak intensities with and without Mn^{2+}, resp.); a higher normalized value indicates a greater degree of line broadening.

ACKNOWLEDGMENTS. We thank Jay Stasser for help with fitting XAS data, Markos Koutmos for discussions and metal site modeling, and the Michigan Economic Development Corporation and the Michigan Technology Tri-Corridor for support of the purchase of the 600 MHz spectrometer. This work is supported by National Institutes of Health Al 66975 (to H.M.A-H), GM 38047 (to J.E.P-H.), GM 55387 (to C.A.F.), and T32 GM08353 (to K.S.K.).

1. Woodson SA (2005) Metal ions and RNA folding: a highly charged topic with a dynamic future. *Curr Opin Chem Biol*, 9:104–109.
2. Sigel RK, Pyle AM (2007) Alternative roles for metal ions in enzyme catalysis and the implications for ribozyme chemistry. *Chem Rev*, 107:97–113.
3. Harris ME, Christian EL (2003) Recent insights into the structure and function of the ribonucleoprotein enzyme ribonuclease P. *Curr Opin Struct Biol*, 13:325–333.
4. Smith JK, Hsieh J, Fierke CA (2007) Importance of RNA-protein interactions in bacterial ribonuclease P structure and catalysis. *Biopolymers*, 87:329–338.
5. Beebe JA, Kurz JC, Fierke CA (1996) Magnesium ions are required by Bacillus subtilis ribonuclease P RNA for both binding and cleaving precursor $tRNA^{Asp}$. *Biochemistry*, 35:10493–10505.
6. Cassano AG, Anderson VE, Harris ME (2004) Analysis of solvent nucleophile isotope effects: evidence for concerted mechanisms and nucleophilic activation by metal coordination in nonenzymatic and ribozyme-catalyzed phosphodiester hydrolysis. *Biochemistry*, 43:10547–10559.
7. Kurz JC, Fierke CA (2002) The affinity of magnesium binding sites in the Bacillus subtilis RNase P x pre-tRNA complex is enhanced by the protein subunit. *Biochemistry*, 41:9545–9558.
8. Misra VK, Draper DE (1998) On the role of magnesium ions in RNA stability. *Biopolymers*, 48:113–135.
9. Cuzic S, Hartmann RK (2005) Studies on Escherichia coli RNase P RNA with Zn2+ as the catalytic cofactor. *Nucleic Acids Res*, 33:2464–2474.
10. Frank DN, Pace NR (1998) Ribonuclease P: Unity and diversity in a tRNA processing ribozyme. *Annu Rev Biochem*, 67:153–180.
11. Torres-Larios A, Swinger KK, Krasilnikov AS, Pan T, Mondragon A (2005) Crystal structure of the RNA component of bacterial ribonuclease P. *Nature*, 437:584–587.
12. Rasmussen TA, Nolan JM (2002) G350 of Escherichia coli RNase P RNA contributes to Mg^{2+} binding near the active site of the enzyme. *Gene*, 294:177–185.
13. Frank DN, Pace NR (1997) In vitro selection for altered divalent metal specificity in the RNase P RNA. *P Natl Acad Sci USA*, 94:14355–14360.
14. Crary SM, Kurz JC, Fierke CA (2002) Specific phosphorothioate substitutions probe the active site of Bacillus subtilis ribonuclease P. *RNA*, 8:933–947.
15. Christian EL, Kaye NM, Harris ME (2000) Helix P4 is a divalent metal ion binding site in the conserved core of the ribonuclease P ribozyme. *RNA*, 6:511–519.
16. Harris ME, Pace NR (1995) Identification of phosphates involved in catalysis by the ribozyme RNase P RNA. *RNA*, 1:210–218.
17. Christian EL, Smith KM, Perera N, Harris ME (2006) The P4 metal binding site in RNase P RNA affects active site metal affinity through substrate positioning. *RNA*, 12:1463–1467.
18. Kazantsev AV, Krivenko AA, Pace NR (2009) Mapping metal-binding sites in the catalytic domain of bacterial RNase P RNA. *RNA*, 15:266–276.
19. Getz MM, Andrews AJ, Fierke CA, Al-Hashimi HM (2007) Structural plasticity and Mg2+ binding properties of RNase P P4 from combined analysis of NMR residual dipolar couplings and motionally decoupled spin relaxation. *RNA*, 13:251–266.
20. Smith D, Burgin AB, Haas ES, Pace NR (1992) Influence of metal ions on the ribonuclease P reaction. Distinguishing substrate binding from catalysis. *J Biol Chem*, 267:2429–2436.
21. Brannvall M, Kirsebom LA (2001) Metal ion cooperativity in ribozyme cleavage of RNA. *P Natl Acad Sci USA*, 98:12943–12947.
22. Wedekind JE, McKay DB (2003) Crystal structure of the leadzyme at 1.8 Å resolution: Metal ion binding and the implications for catalytic mechanism and allo site ion regulation. *Biochemistry*, 42:9554–9563.
23. Ennifar E, et al. (1999) The crystal structure of the dimerization initiation site of genomic HIV-1 RNA reveals an extended duplex with two adenine bulges. *Structure*, 7:1439–1449.
24. Penner-Hahn JE (2005) Characterization of "spectroscopically quiet" metals in biology. *Coordin Chem Rev*, 249:161–177.
25. Hitchcock AP, Lock CJL, Pratt WMC (1982) EXAFS studies of a Pt-dimer—DNA complex. *Inorg Chim Acta*, 66:L45–47.
26. Smirnov IV, Kotch FW, Pickering IJ, Davis JT, Shafer RH (2002) Pb EXAFS studies on DNA quadruplexes: Identification of metal ion binding site. *Biochemistry*, 41:12133–12139.
27. Cowan JA (1993) Metallobiochemistry of RNA. $Co(NH_3)_6^{(3+)}$ as a probe for $Mg^{2+}(aq)$ binding sites. *J Inorg Biochem*, 49:171–175.
28. Schmitz M, Tinoco I Jr (2000) Solution structure and metal-ion binding of the P4 element from bacterial RNase P RNA. *RNA*, 6:1212–1225.
29. Wild K, Weichenrieder O, Leonard GA, Cusack S (1999) The 2 Å structure of helix 6 of the human signal recognition particle RNA. *Structure*, 7:1345–1352.
30. Markley JC, Godde F, Sigurdsson ST (2001) Identification and characterization of a divalent metal ion-dependent cleavage site in the hammerhead ribozyme. *Biochemistry*, 40:13849–13856.
31. Ye JD, et al. (2008) Synthetic antibodies for specific recognition and crystallization of structured RNA. *P Natl Acad Sci USA*, 105:82–87.
32. Thorp HH (1992) Bond valence sum analysis of metal-ligand bond lengths in metalloenzymes and model complexes. *J Inorg Chem*, 31:1585–1588.
33. Milligan JF, Uhlenbeck OC (1989) Synthesis of small RNAs using T7 RNA polymerase. *Methods Enzymol*, 180:51–62.
34. Tobin DA, Pickett JS, Hartman HL, Fierke CA, Penner-Hahn JE (2003) Structural characterization of the zinc site in protein farnesyltransferase. *J Am Chem Soc*, 125:9962–9969.
35. Weng TC, Waldo GS, Penner-Hahn JE (2005) A method for normalization of X-ray absorption spectra. *J Synchrotron Radiat*, 12:506–510.
36. McMaster WH, Del Grande NK, Mallet JH, Hubbell JH (1969) X-ray cross sections, U.S.Dept. of Commerce.
37. Clark-Baldwin K, et al. (1998) The limitations of X-ray absorption spectroscopy for determining the structure of zinc sites in proteins. When is a tetrathiolate not a tetrathiolate?. *J Am Chem Soc*, 120:8401–8409.
38. Zabinsky SI, Rehr JJ, Ankudinov A, Albers RC, Eller MJ (1995) Multiple-scattering calculations of x-ray-absorption spectra. *Phys Rev B*, 52:2995–3009.
39. George GN, Pickering IJ (1993) *EXAFSPAK* (Stanford University, Palo Alto, CA).
40. McClure CP, et al. (2003) EXAFS studies of the zinc sites of UDP-(3-O-acyl)-N-acetylglucosamine deacetylase (LpxC). *J Inorg Biochem*, 94:78–85.
41. Meissner A, Sorensen OW (1999) Optimization of three-dimensional TROSY-type HCCH NMR correlation of aromatic (1)H-(13)C groups in proteins. *J Magn Reson*, 139:447–450.
42. Meissner A, Duus JO, Sorensen OW (1997) Integration of spin-state-selective excitation into 2D NMR correlation experiments with the heteronuclear ZQ/2Q pi rotations for 1JXH- resolved E.COSY-type measurements of heteronuclear coupling constants in proteins. *J Biomol NMR*, 10:89–94.
43. Delaglio F, et al. (1995) NMRPipe: Amultidimensional spectral processing system based on UNIX pipes. *J Biomol NMR*, 6:277–293.
44. Johnson BA, Stevens SP, Williamson JM (1994) Determination of the three-dimensional structure of margatoxin by 1H, 13C, 15N triple-resonance nuclear magnetic resonance spectroscopy. *Biochemistry*, 33:15061–15070.